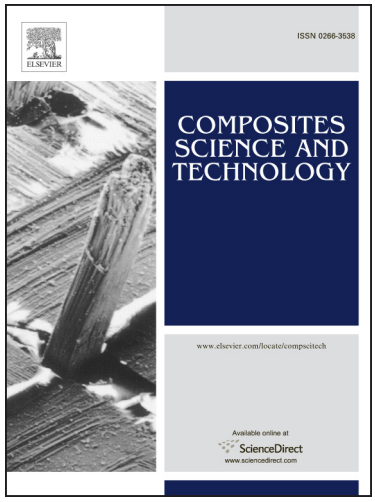

Visualization of the conductive paths in injection moulded MWNT/polycarbonate nanocomposites by conductive AFM

Bernadeth Kiss-Pataki, Jyri Tiusanen, Gergely Dobrik, Zofia Vértesy, Zsolt Endre Horváth

PII: S0266-3538(13)00416-8
DOI: http://dx.doi.org/10.1016/j.compscitech.2013.10.016
Reference: CSTE 5651

To appear in: *Composites Science and Technology*

Received Date: 18 July 2013
Revised Date: 5 September 2013
Accepted Date: 27 October 2013

Please cite this article as: Kiss-Pataki, B., Tiusanen, J., Dobrik, G., Vértesy, Z., Horváth, Z.E., Visualization of the conductive paths in injection moulded MWNT/polycarbonate nanocomposites by conductive AFM, *Composites Science and Technology* (2013), doi: http://dx.doi.org/10.1016/j.compscitech.2013.10.016

Visualization of the conductive paths in injection moulded MWNT/polycarbonate nanocomposites by conductive AFM

Bernadeth Kiss-Pataki[a,*], Jyri Tiusanen[b], Gergely Dobrik[a], Zofia Vértesy[a], Zsolt Endre Horváth[a]

[a] *Institute for Technical Physics and Materials Science, Research Centre for Natural Sciences, Hungarian Academy of Sciences, Konkoly Thege Miklós Rd. 29–33, 1121 Budapest, Hungary*

[b] *Promolding B.V., Laan van Ypenburg, 2497 GB The Hague, The Netherlands*

[*] *Corresponding Author: pataki.bernadeth@ttk.mta.hu*

Tel. +36-1-392-2680; Fax.: +36-1-392-2226

Abstract

Electrical conductivity of MWNT filled polymer composites can strongly depend on the dispersion of the filler. Injection moulding of the same nanotube filled conductive composite materials can lead to significant differences in conductivities while the corresponding morphological changes seem to be moderate. Here we report on a conductive atomic microscopy (C-AFM) study of a series of polycarbonate/MWNT settings injection moulded with different injection speeds and melt temperatures, completed with optical microscopy, SEM and TEM characterization. C-AFM was found to be able to visualize the significant differences in the morphology of electrical pathways in cross section. These morphological variations seem to correlate to the differing volume resistivity data and are in agreement with the expected structural effects of injection moulding processes with different parameters.

Keywords: A Polymer-matrix composites (PMCs) **A** Carbon nanotubes, **B** Electrical properties, **D** Atomic force microscopy (AFM), **E** Injection moulding

1. Introduction

Since Iijima [1] identified multi-walled carbon nanotubes (MWNT) in 1991 and single wall carbon nanotubes (SWNT) along [2] with Bethune [3] in 1993, scientists' attention was kindled by their outstanding properties. Features of CNTs such as excellent mechanical properties, electrical and thermal conductivity associated with their high aspect ratio and low density, have several potential benefits which are expected to manifest when they are employed as fillers in polymers [4–20].

Practical methods are available; allowing to study and understand the relationship between the microstructure and macroscopic mechanical properties of MWNT/polymer composites. Dealing with electrically conducting MWNT nanocomposites, a similar multiscale characterization should be completed with the high-resolution mapping of the electrical properties. Though the strong correlation of the nanoscale morphology and the electrical properties is apparent, conventional microscopic methods as transmission optical microscopy (TOM), scanning electron microscopy (SEM), and transmission electron microscopy (TEM) provide only indirect information on the electrical properties.

One of the possible solutions is offered by an SEM based method: charge contrast imaging (CCI), which is able to differentiate between the nanotubes connected to the electrical network. The CCI method is based on the fact that in case of certain SEM imaging conditions the nanotubes connected to electrical percolation paths, have different contrast to nanotubes not connected to it [20]. A. Noll and T. Burkhart characterized the electrical conductivity of multiwall carbon nanotubes poly(p-phenilene sulphide) composite using CCI of a low acceleration voltage SEM, revealing the electrical properties of the studied composite [18,19]. Socher et al reportedly used SEM-CCI to visualize the dispersion structure and the conductive network of 2 wt.% CNT containing PA12 composites [21]. Formerly Jeon et al accessed the

dispersion of SWCNTs in crystalline iPP matrix with increasing SWCNT content by CCI SEM as well [22]. Even though CCI method is a very powerful tool for imaging which nanotubes contributes to the electrical percolation, the charge transport induced by accelerated electrons differs from the processes which occur during a usual I-V resistivity measurement. On the other hand the image is a projection of the volume mapped by the electrons from the estimated thickness of 300 Å at 30 kV [23,24].

Conductive tip atomic force microscopy (C-AFM) as the member of the family of scanning probe microscopies, images directly the local electrical conductance of the studied sample. The principle of the method is that a conductive tip is used for scanning the sample surface in contact AFM mode [25–27]. A voltage is applied between the tip and the sample generating a current which is registered pixel by pixel together with the topographic information from the same area of the sample. The main advantage of C-AFM over standard electrical measurement techniques is the high spatial resolution. Its full potential might be exploited in mapping the conductance of a surface only when the conductive objects present in the sample and on its surface are connected to the below electrode in order to allow the charge transport through the whole thickness of the sample [28]. The C-AFM method has been used in characterizing the local electric properties of wide area of samples, e.g. in case of photovoltaic fullerene blends [29] and organic films [40–43], but no reports have shown its use in study of MWNT/polymer composites.

The aim of this work is to demonstrate the capability, illustrate the sort of achievable information and assess the reliability of the application of the C-AFM method in studying the local electrical properties of MWNT/polymer composites. Hence a comparative study was performed between C-AFM and TOM, SEM, TEM methods to investigate six 3 wt. % MWNT/polycarbonate injection moulding settings with diverse electrical volume resitivities.

Injection moulded parts were produced using a 3wt. % polycarbonate raw material varying the melt temperature (t_m) and the injection speed (i_v). The use of MWNT based nanocomposites for commercial applications needs an understanding of how the processing conditions influence the arrangement of nanotubes in the matrix and the morphology of the electrical percolation network which subsequently determines the nanocomposites' final electrical properties.

2. Experimental

2.1. Composite processing

The materials subjected to our investigations were injection moulded from polycarbonate (PC) filled with 3 wt. % of MWNT. The raw material was obtained diluting a Platicyl^{TM} PC1501 masterbatch by Lexan 123R Resin Polycarbonate by melt compounding in a twin screw extruder, with a screw speed of 590 rpm and a throughput of 11 kg/h and a cylinder temperature of 240 °C. The PC1501 was produced by Nanocyl using 15 wt. % NC7000 type of multi-wall carbon nanotubes and polycarbonate [34]. The MWNTs were produced by catalytic chemical vapour deposition by Nanocyl. They have reportedly an average diameter of 9.5 nm, average length of 1.5 μm and a surface area of 250-300 m^2/g.

Using an Engel ES 330/80 HLS horizontal injection moulding machine, 76 mm long and wide and 4 mm thick parts were injection moulded from the above described raw material. The mould had a 67.5 mm wide film gate with 1mm opening. Six different process parameter settings were used to produce 25 plates of each, using different melt temperatures (T_m) and injection velocities (i_v), see Table 1.

Sample preparation for characterization

Figure 1. shows an injection moulded plate and the steps of the sample preparation procedure. A bar was removed from the middle of the plate, and then further slices were microtomed by a diamond knife in the direction perpendicular to the flow direction using a Leica

Ultracut microtome, cutting 5μm thick slices for optical microscopy and 70-100 nm thin slices for TEM. The masterbatch and the raw material, available as granules was embedded in epoxy resin, and then cut as the injection moulded sample bars. A part of approx. 5 mm thickness with the mirror flat surface left over, that's back side was fixed to a stainless steel sample holder by carbon paste. C-AFM and SEM investigations were performed using this sample. The composite piece was then removed from the sample holder, the carbon paint was cleaned away by sandpaper and the two opposite sides perpendicular to the injection direction were contacted with silver paint for volume resistivity measurements.

2.3. Characterization

Electrical volume resistivity (ρ) measurements were carried out with a two wire method using a Keithley 2100 digital multimeter, the measurements were repeated until a constant value was obtained (see further details in [35]).

Optical microscopy observation was completed using an Olympus BH2 transmission optical microscope with a Leica DFC 280 digital camera. We determined the macrodispersion index of the samples following the method described by S. T. Buschhorn et al., and G. R. Kasaliwal et al. [10,36] calculated and averaged on ten images for each sample. The macrodispersion index (D), considers the area occupied by filler divided by the total investigated area on a bitmap of the transmission optical microscopy image, and was calculated using the formula: $D=[1-f((A_{CNT}/A_0)/v)]*100\%$, where f is a factor keeping in view the density of CNT agglomerates, that's value, was estimated to be 0.25. This may have inaccuracies due to inhomogeneity of the slice' thickness [37,38] as well as the volume of the carbon nanotubes, which was considered by the notation v in the above formula. A_{CNT} (with size ›1μm were neglected) is the area occupied by the carbon nanotubes, while A_0 is the total investigated area. The density of CNTs 1.75 g/cm^3 was assumed [36,38].

Scanning electron microscopy was performed by a LEO 1540XB field emission scanning electron microscope (FESEM) equipped with InLens and Everhart-Thornley secondary electron detectors used at 5 kV EHT.

Transmission electron microscopy (TEM) investigation was carried out on a Philips CM20 transmission electron microscope fitted with LaB_6 electron gun and operated at 200 kV.

Conductive Atomic Force Microscopy (C-AFM) investigations were performed using a Multimode 8 AFM (Bruker) operated with 20 nm Pt-Ir coated AFM probes in the C-AFM mode to capture the conductive AFM images, setting the following parameters under ambient conditions and room temperature: 100 pA current sensitivity and 100 mV DC sample bias voltage, in 10μm scanning area, with 512x512 pixel resolutions. In this case the size of one pixel is about 20 nm, which is commensurable with the diameter of the applied MWNTs and is in the order of magnitude of the probes radius of curvature. The maximum current values measured ranged between 2.8 nA and 0.51μA. Regarding that C-AFM scans dangling tubes on the surface, pulled out during the sample preparation process, the tip contacts not only the tubes' end but their length might also be imaged due to bending. These effects result in a blurred image of the individual tubes. Considering the fact that C-AFM images solely the surface without any insight, the image of an originally electrically connected MWNT cluster may be displayed as separated but close spots. The investigations at the nano scale carry some difficulties, among them one might take into account that the samples surface may be damaged, due to strong forces applied by the tip in contact mode [33], but the tip could abrade or might collect contamination from the samples surface, therefore fulfilling the requirement of a clean and flat surface will ensure proper AFM investigations.

3. Results and discussion

Volume resistivity study of the samples (Table 1) showed high variation of the volume resistivity values ranging from 2.23 to 1470 kΩ*cm. As a first attempt transmission optical microscopy was carried out following the usual analysis route mentioned above to brighten the morphological reasons of the significant differences found. Fig.2. shows two typical examples of micrographs. The macrodispersion index (D) data of the investigated samples displayed in Table 1. shows values ranging between 99.84-99.97% of evenly distributed filler at the macro scale. Besides, the values of the individual samples are fairly close to each other proving that the different applied processes have not modified the morphology distinctively at the macro scale.

3.1. Scanning electron microscopy (SEM) of the samples with the highest (F2) and lowest (F6) volume resistivity values have been performed and their SEM images are presented on Figure 3. The greyish background is considered as the matrix material, in this case polycarbonate, while the white stringy objects are the MWNTs. Both samples present a porous, spongy structure with cavities of a few hundred nanometers size. Sample F6 showed more uncovered nanotubes, while sample F2 proved better wetting of the tubes (compare Figs. 3A and B).

3.2. TEM investigations of the six injection moulding settings resulted samples and the masterbatch with 15wt. % CNT content besides the raw material used for injection moulding containing 3 wt. % MWNTs were also performed. On the TEM micrographs displayed in Fig. 4 individual nanotubes, their clusters and areas of neat polymer are clearly recognizable. Besides, a few irregular carbon particles are also visible in some of the images presumably they are impurities of the MWNT raw material. All the images include parallel bands due to the common defects of the used diamond knife. Assessing the distribution of MWNTs in the 15 wt. % masterbatch (MB) sample is demanding due to their high density. The presence of neat polymer areas on the left side of the image however implies the non-uniform distribution of the filler.

After dilution, the 3wt. % raw material sample shows a few microns size connected clusters separated by almost neat polymer. As a result of injection moulding, clear structural changes were noticed on all of the samples, which affected the distribution of the MWNTs in different degrees. The image of sample F1 shows the most uniformly dispersed MWNTs forming clusters scarcely. The volume fraction of neat polymer parts seems to be very low. Sample F2 has mainly evenly dispersed MWNTs and loose clusters with neater polymer islands. Sample F3 has uniformly dispersed loose elongated shape MWNT clusters being denser than in case of F2. In case of sample F4 compared to F3, the MWNTs form clusters but the areas between them contain individual nanotubes [39]. The image of sample F5 shows mainly small MWNT clusters divided by areas containing individual tubes with varied density. Sample F6 displays elongated MWNT clusters, located as interconnected parallel cluster groups. In general, these changes observed after injection moulding of the raw material resulted in more uniform textures.

3.3. Figure 4. presents the C-AFM images of the investigated sample series. Regarding the peculiarity of the sample that the conductance is due to the presence of the nanotubes, while the polymer matrix is insulating, obviously even the smallest measured current indicates the presence of MWNTs connected to the electrical percolation network. Therefore we found it practical to visualize the conductance of the samples on a black and white figure where the white parts belong to conductive paths, while the black ones are associated to the insulating parts of the sample. Information loss may occur due to this binarization but one should take notice of that C-AFM is not suitable for quantitative information retrieval anyway. This speciality of the method was verified e.g. by Andrejs et al. on investigating donor-doped lead-zirconate -titanate layers [50], and Lang et al when characterizing Al_2O_3 films [41]. Our experiences confirmed that even though successive measurements are performed in the same area using the same probe with the same parameters, deviations by a factor of two in the current values were observed, still resulting

in quite satisfactory qualitative morphological similarities between the images (not shown here). Among the different factors responsible for the quantitative uncertainty of the method, a significant one is the unstable contact. At each pixel, the surface is pressed by the sharp probe exerting a finite force, which deforms the material to a certain extent. Two components might be distinguished during the probe-sample contact interaction; an elastic and a surface dominated one, the later originates e.g. from the Van der Waals interactions [39]. Omitting all but the elastic interaction, we made an estimation of the contact area using Sneddon's model [39,42]. Spherical tip shape with 40 nm radius and a perfectly elastic sample material with the macroscopic elastic parameters; E = 2.8 GPa Young's modulus and ν= 0.35 Poisson's ratio were assumed. The spring constant of the cantilever was determined and calibrated in situ from its vibration properties using the dedicated routine of the device. The interaction force can be determined for each scan as the relationship between the electric signal of the feedback system, dedicated to keep the cantilever bending constant and the real geometrical situation is well known. In our case it was F = 80 ±15 nN, that allowed the radius of the contact area to be calculated obtaining a = 9 ± 3nm. The random distribution of MWNTs and the spongy, porous morphology of the sample surfaces revealed by SEM study implies a pixel by pixel variation of the sample deformation, causing of the contact area and consequently the flowing current changes as well [41]. Instabilities between the feedback signal and the interaction force due to thermal drifts; nonlinearities of the piezoelectric actuators may induce apparent changes. Even though the tip may keep conducting for several measurement hours its attrition occurs inevitably leading to the change of its shape. Another effect of the tip-sample interaction induced sample deformation is the relative shift of the MWNTs within the sample, by modifying the resistance of the conductive path next to the investigated spot. One may note that the resistance of a CNT network is determined by the

resistance of the CNT-CNT junctions [43]. Considering the above mentioned effects, quantitative assessments of C-AFM measurements is highly unadvised.

Figure 5.F1 displays the C-AFM image of the used raw material; featuring conductive spots exceeding typically the size of 150 – 250 nm. These spots situated mostly in groups separated by insulating islands can be attributed to the dense parts of MWCNT clusters visible in the corresponding TEM image (Fig. 4.F1-Fx). The injection moulding settings of sample F1 was 280 C^0 melt temperature and 18 mm/s injection speed, i.e. medium shear was expected, which is known to enhance the dispersion of the nanotubes [35]. C-AFM image of the sample presents conductive spots with significantly smaller average size and increased dispersion, the average area of continuous insulating areas is reduced. The overall coverage by conductive spots is 2.63% of the imaged area. In agreement with the picture the C-AFM data indicates, TEM image of the same sample (Fig 5-F1) shows much more scattered MWNT distribution with only smaller, low density clusters. Sample F2 was produced using the same 280 C^0 melt temperature as in case of sample F1 but it had a higher injection speed of 42 mm/s. Therefore a higher shear is expected, dispersing and separating the nanotubes. What we see in the C-AFM image of this sample is that the overall coverage is really low, only 0.75% of the imaged area. Scarce but relatively extended and grouped conductive areas separated by large insulating domains are present. Based on the corresponding TEM results we can suppose that most of the MWNT clusters have been segregated to separated nanotubes or isolated from the conductive network, only a few of them remained in contact. Sample F3 was processed using 6 mm/s injection speed combined with a higher melt temperature; 300 C^0. C-AFM revealed that 15.85% of the studied area is conductive, the conductive spots are smaller than in case of the raw material but they form dense, elongated clusters in accord with the corresponding TEM image (Fig.4.F3). Here we can suppose that the nanotube clusters of the raw material have been loosen, expanded as a consequence of the higher

mobility of polymer chains at elevated melt temperature, while the CNT-CNT contacts were not broken for lack of significant shear. Turning to samples F4 and F5 processed at the same temperature but with higher injection speeds, 30 and 42 mm/s, respectively, the individual conductive spots show similar shape and approximate size but the density and size of their groups are decreasing as injection speed increases. The coverage of the conductive spots is 5.88% and 2.35% for samples F4 and F5, respectively. Here we see how the morphology characteristic for sample F3 has been changed by the effect of moderate and high sheer: a part of the MWNT clusters have been dispersed and separated from the conducting network, higher extent in case of sample F5. TEM study of the F3, F4 and F5 samples confirms the previous picture: extended, loose MWNT clusters are present in sample F3 with empty polymer areas between them. TEM image of sample F5 presents smaller clusters and significant decrease of the empty polymer islands. TEM of sample F4 shows a somewhat intermediate structure but this cannot easily be recognized because of the higher slice thickness. A very high 320 C^0 melt temperature was linked to a 42 mm/s high injection speed in case of sample F6. Compared to F3, here we can notice also the presence of bigger conductive spots though most of them are still small and densely packed. They cover 10 % of the imaged area of sample F6. Despite the high injection speed, the sheer in case of this high temperature was not high enough to significantly disperse the nanotubes. On the contrary, the increased mobility of the polycarbonate chains eased the build-up of new, larger conductive spots with different shape compared to the raw material. Both elongated clusters and some dense areas can be recognized in the corresponding TEM image.

The coverage by conductive spots compared to the bulk electrical resistivity data (see Table 1.) of samples produced using the same melt temperature prevails the tendency: the larger coverage matches a lower volume resistivity value. This tendency seems not to be valid for samples with different melt temperatures.

Conclusions

To the best of our knowledge for the first time C-AFM was used to map the electrical properties MWNT/polycarbonate composites. Significant differences in the morphology of electrical pathways in cross section were revealed, which seem to correspond to the expected structural effects of the used injection moulding settings and the various volume resistivity data. Particularly we observed the variation of the density of the MWNT clusters under the mobility of the polymer chains; besides we proved that the increasing shear disperses the MWNTs and disrupts their connection to the electrical network. C-AFM maps are in accord with the result obtained by transmission optical microscopy, SEM, and TEM. It stands also for proof that the C-AFM might contribute to a more comprehensive understanding of structure-property relationship for electrically conductive composites.

Acknowledgements

This work was funded by the European Community's Seventh Framework Program (FP7/2007-2013) under grant agreement no. 238363. The authors also wish to thank Péter Nemes-Ince (MTA TTK MFA, Budapest) for his helpful advices related to conductive atomic force microscopy investigation. We would also like to thanks Anna Matveeva and Dr. Ferrie van Hattum, (University of Minho, Guimaraes) for their advices.

References

[1] S. Iijima, Helical microtubules of graphitic carbon, Letters of Nature. 354 (1991) 56–58.

[2] S. Iijima, Single-shell carbon nanotubes of 1-nm diameter, Nature. 363 (1993) 603–605.

[3] D.S. Bethune, C.H. Klang, M.S. de Vries, G. Gorman, R. Savoy, J. Vazquez, et al., Cobalt-catalysed growth of crabon nanotubes with single-atomic-layer walls, Nature. 363 (1993) 605–607.

[4] T. Villmow, B. Kretzschmar, P. Pötschke, Influence of screw configuration, residence time, and specific mechanical energy in twin-screw extrusion of polycaprolactone/multi-

walled carbon nanotube composites, Composites Science and Technology. 70 (2010) 2045–2055.

[5] S. Abbasi, P.J. Carreau, A. Derdouri, Flow induced orientation of multiwalled carbon nanotubes in polycarbonate nanocomposites: Rheology, conductivity and mechanical properties, Polymer. 51 (2010) 922–935.

[6] M. Abdel-Goad, P. Pötschke, Rheological characterization of melt processed polycarbonate-multiwalled carbon nanotube composites, Journal of Non-Newtonian Fluid Mechanics. 128 (2005) 2–6.

[7] O. Meincke, D. Kaempfer, H. Weickmann, C. Friedrich, M. Vathauer, H. Warth, Mechanical properties and electrical conductivity of carbon-nanotube filled polyamide-6 and its blends with acrylonitrile/butadiene/styrene, Polymer. 45 (2004) 739–748.

[8] G. Hu, C. Zhao, S. Zhang, M. Yang, Z. Wang, Low percolation thresholds of electrical conductivity and rheology in poly(ethylene terephthalate) through the networks of multi-walled carbon nanotubes, Polymer. 47 (2006) 480–488.

[9] I. Alig, D. Lellinger, S.M. Dudkin, P. Pötschke, Conductivity spectroscopy on melt processed polypropylene–multiwalled carbon nanotube composites: Recovery after shear and crystallization, Polymer. 48 (2007) 1020–1029.

[10] S.T. Buschhorn, M.H.G. Wichmann, J. Sumfleth, K. Schulte, S. Pegel, G.R. Kasaliwal, et al., Charakterisierung der Dispersionsgüte von Carbon Nanotubes in Polymer-Nanokompositen, Chemie Ingenieur Technik. 83 (2011) 767–781.

[11] T. Belin, F. Epron, Characterization methods of carbon nanotubes: a review, Materials Science and Engineering: B. 119 (2005) 105–118.

[12] S. Sathyanarayana, G. Olowojoba, P. Weiss, B. Caglar, B. Pataki, I. Mikonsaari, et al., Compounding of MWCNTs with PS in a Twin-Screw Extruder with Varying Process Parameters: Morphology, Interfacial Behavior, Thermal Stability, Rheology, and Volume Resistivity, Macromolecular Materials and Engineering. 298 (2013) 89–105.

[13] K. Cheah, M. Forsyth, G.P. Simon, Conducting composite using an immiscible polymer blend matrix, Synthetic Metals. 102 (1999) 1232–1233.

[14] G. Olowojoba, S. Sathyanarayana, B. Caglar, B. Kiss-Pataki, I. Mikonsaari, C. Hübner, et al., Influence of process parameters on the morphology, rheological and dielectric properties of three-roll-milled multiwalled carbon nanotube/epoxy suspensions, Polymer. 54 (2013) 188–198.

[15] S. Pegel, P. Pötschke, G. Petzold, I. Alig, S.M. Dudkin, D. Lellinger, Dispersion, agglomeration, and network formation of multiwalled carbon nanotubes in polycarbonate melts, Polymer. 49 (2008) 974–984.

[16] I. Alig, T. Skipa, D. Lellinger, P. Pötschke, Destruction and formation of a carbon nanotube network in polymer melts: Rheology and conductivity spectroscopy, Polymer. 49 (2008) 3524–3532.

[17] T. Villmow, S. Pegel, P. Potschke, U. Wagenknecht, P. Pötschke, Influence of injection molding parameters on the electrical resistivity of polycarbonate filled with multi-walled carbon nanotubes, Composites Science and Technology. 68 (2008) 777–789.

[18] A. Noll, T. Burkhart, Morphological characterization and modelling of electrical conductivity of multi-walled carbon nanotube/poly(p-phenylene sulfide) nanocomposites obtained by twin screw extrusion, Composites Science and Technology. 71 (2011) 499–505.

[19] W. Ding, A. Eitan, F.T. Fisher, X. Chen, D.A. Dikin, R. Andrews, et al., Direct Observation of Polymer Sheathing in Carbon Nanotube−Polycarbonate Composites, Nano Letters. 3 (2003) 1593–1597.

[20] J. Loos, N. Grossiord, C.E. Koning, O. Regev, On the fate of carbon nanotubes: Morphological characterisations, Composites Science and Technology. 67 (2007) 783–788.

[21] R. Socher, B. Krause, R. Boldt, S. Hermasch, R. Wursche, P. Pötschke, Melt mixed nano composites of PA12 with MWNTs: Influence of MWNT and matrix properties on macrodispersion and electrical properties, Composites Science and Technology. 71 (2011) 306–314.

[22] K. Jeon, S. Warnock, C. Ruiz-Orta, A. Kismarahardja, J. Brooks, R.G. Alamo, Role of matrix crystallinity in carbon nanotube dispersion and electrical conductivity of iPP-based nanocomposites, Journal of Polymer Science Part B: Polymer Physics. 48 (2010) 2084–2096.

[23] K.T. Chung, J.H. Reisner, E.R. Campbell, Charging phenomena in the scanning electron microscopy of conductor-insulator composites: A tool for composite structural analysis, Journal of Applied Physics. 54 (1983) 6099.

[24] J. Loos, A. Alexeev, N. Grossiord, C.E. Koning, O. Regev, Visualization of single-wall carbon nanotube (SWNT) networks in conductive polystyrene nanocomposites by charge contrast imaging., Ultramicroscopy. 104 (2005) 160–7.

[25] G. Binnig, C.F. Quate, C. Gerber, Atomic force microscope.pdf, Physical Review Letters. 56 (1986) 930–933.

[26] D. Rugar, P. Hansma, Atomic force microscopy, Physics Today. (1990) 23–30.

[27] E. Meyer, Atomic force microscopy, Progress in Surface Science. 41 (1992) 3–49.

[28] L. Zhang, T. Sakai, N. Sakuma, T. Ono, K. Nakayama, Nanostructural conductivity and surface-potential study of low-field-emission carbon films with conductive scanning probe microscopy, Applied Physics Letters. 75 (1999) 3527.

[29] A. Alexeev, J. Loos, M.M. Koetse, Nanoscale electrical characterization of semiconducting polymer blends by conductive atomic force microscopy (C-AFM)., Ultramicroscopy. 106 (2006) 191–9.

[30] J. Ravier, F. Houze, F. Carmona, O. Schneegans, H. Saadaoui, Mesostructure of polymer / carbon black composites observed by conductive probe atomic force microscopy, Carbon. 39 (2001) 314–318.

[31] H. Tajima, T. Shimada, K. Sawasaki, S. Umemura, S. Hirono, S. Tsuchitani, et al., Nanoscale electric modification and observation of sputtered carbon films by atomic force microscopy with conductive tip, Surface and Coatings Technology. 169-170 (2003) 208–210.

[32] M. Knite, V. Teteris, B. Polyakov, D. Erts, Electric and elastic properties of conductive polymeric nanocomposites on macro- and nanoscales, Materials Science and Engineering: C. 19 (2002) 15–19.

[33] A. Vetushka, T. Itoh, Y. Nakanishi, A. Fejfar, S. Nonomura, M. Ledinský, et al., Conductive atomic force microscopy on carbon nanowalls, Journal of Non-Crystalline Solids. 358 (2012) 2545–2547.

[34] Nanocyl, General information., British Journal of Anaesthesia. 110 (n.d.) NP.

[35] J. Tiusanen, D. Vlasveld, J. Vuorinen, Review on the effects of injection moulding parameters on the electrical resistivity of carbon nanotube filled polymer parts, Composites Science and Technology. 72 (2012) 1741–1752.

[36] G.R. Kasaliwal, S. Pegel, A. Göldel, P. Pötschke, G. Heinrich, Analysis of agglomerate dispersion mechanisms of multiwalled carbon nanotubes during melt mixing in polycarbonate, Polymer. 51 (2010) 2708–2720.

[37] T. Villmow, P. Pötschke, S. Pegel, L. Häussler, B. Kretzschmar, Influence of twin-screw extrusion conditions on the dispersion of multi-walled carbon nanotubes in a poly(lactic acid) matrix, Polymer. 49 (2008) 3500–3509.

[38] P.P. Guarav Kasaliwal, Andreas Göldel, Influence of Processing Conditions in Small-Scale Melt Mixing and Compression Molding on the Resistivity and Morphology of Polycarbonate – MWNT Composites, Polymer. 112 (2009) 3494–3509.

[39] B. Cappella, G. Dietler, Force-distance curves by atomic force microscopy, in: Surface Science Reports, 1999: pp. 1–104.

[40] L. Andrejs, H. Oßmer, G. Friedbacher, J. Bernardi, A. Limbeck, J. Fleig, Conductive AFM and chemical analysis of highly conductive paths in DC degraded PZT with Ag / Pd electrodes, Solid State Ionics. 244 (2013) 5–16.

[41] K.M. Lang, D. a. Hite, R.W. Simmonds, R. McDermott, D.P. Pappas, J.M. Martinis, Conducting atomic force microscopy for nanoscale tunnel barrier characterization, Review of Scientific Instruments. 75 (2004) 2726.

[42] I.N. Sneddon, the total depth of penetration of the tip of the punch, and for, Int. J. Engng Sci. 3 (1965) 47–57.

[43] P.N. Nirmalraj, P.E. Lyons, S. De, J.N. Coleman, J.J. Boland, Electrical connectivity in single-walled carbon nanotube networks., Nano Letters. 9 (2009) 3890–5.

Table 1. Injection moulding conditions of the investigated 97 wt. % polycarbonate matrix and 3 wt. % of MWNTs samples, the related volume resistivity data of the bulk sample (ρ_{bulk} kΩcm), the area covered by conductive spots in % (A_{cond}%) and the macrodispersion index (D) with its standard deviation (SD) calculated and averaged on ten images for each sample.

Fig.1. Sample preparation method for electrical volume resistivity, transmission optical microscopy, SEM, TEM and C-AFM investigation of $PC_{97}MWNT_3$ composites.

Fig.2. Transmission optical microscopy images of $PC_{97}MWNT_3$ composites, sample F2 (A) and F6 (B)**.**

Fig. 3. Scanning Electron Microscopy images of samples F2 (T_m=280 C°, V_i= 42mm/s; ρ_{bulk}=4600kΩ*cm) and F6 (T_m=320 C°, V_i= 42mm/s; ρ_{bulk}=80kΩ*cm)

Fig.4. Transmission Electron Microscopy images of the injection molded parts and the related raw material: F1-TEM images of sample (T_m=280 C°, V_i= 18mm/s; ρ_{bulk}=13.5kΩ*cm); F2-TEM images of sample (T_m=280 C°, V_i= 42mm/s; ρ_{bulk}=4600kΩ*cm); F3- TEM image of the sample (T_m=300 C°, V_i= 6mm/s; ρ_{bulk}=2.72kΩ*cm); F4- TEM image of the sample (T_m=300 C°, V_i= 30mm/s; ρ_{bulk}=20.4kΩ*cm); F5-TEM image of the sample (T_m=300 C°, V_i= 42mm/s; ρ_{bulk}=45kΩ*cm); F6-TEM image of the sample (T_m=320 C°, V_i= 42mm/s; ρ_{bulk}=18kΩ*cm); Rm-TEM image of the raw material (3 wt% MWNT-polycarbonate diluted by 15wt% MWNT-polycarbonate masterbatch).

Fig. 5. Conducting Atomic Force Microscopy binarized images of cross sections of the injection molded parts: F1-C-AFM images of sample (T_m=280 C°, V_i= 18mm/s; $_{bulk}$=13.5kΩ*cm); F2-C-AFM images of sample (T_m=280 C°, V_i= 42mm/s; ρ_{bulk}=4600kΩ*cm); F3- C-AFM image of the sample (T_m=300 C°, V_i= 6mm/s; ρ_{bulk}=2.72kΩ*cm); F4- C-AFM image of the sample (T_m=300 C°, V_i= 30mm/s; ρ_{bulk}=20.4kΩ*cm); F5-C-AFM image of the sample (T_m=300 C°, V_i= 42mm/s; ρ_{bulk}=45kΩ*cm); F6-C-AFM image of the sample (T_m=320 C°, V_i= 42mm/s; ρ_{bulk}=18kΩ*cm); Rm-C-AFM image of the raw material (3 wt% MWNT-polycarbonate diluted by 15wt% MWNT-polycarbonate masterbatch).

Sample Name	Melt Temperature (C^0)	Injection Velocity (mm/s)	ρ_{bulk} (Ω^*cm)	$\pm SD_{\rho bulk}$	A_{cond}%	D (%)±SD
F1	280	18	2.49E+04	1.4E+03	2.63	99.84±0.14
F2	280	42	4.60E+06	1.1E+06	0.75	99.94±0.013
F3	300	6	6.79E+03	1.7E+02	15.85	99.92±0.05
F4	300	30	4.08E+04	8.4E+02	5.88	99.97±0.007
F5	300	42	1.35E+05	5.1E+03	2.35	99.91±0.06
F6	320	42	8.00E+04	3.8E+03	10	99.92±0.05

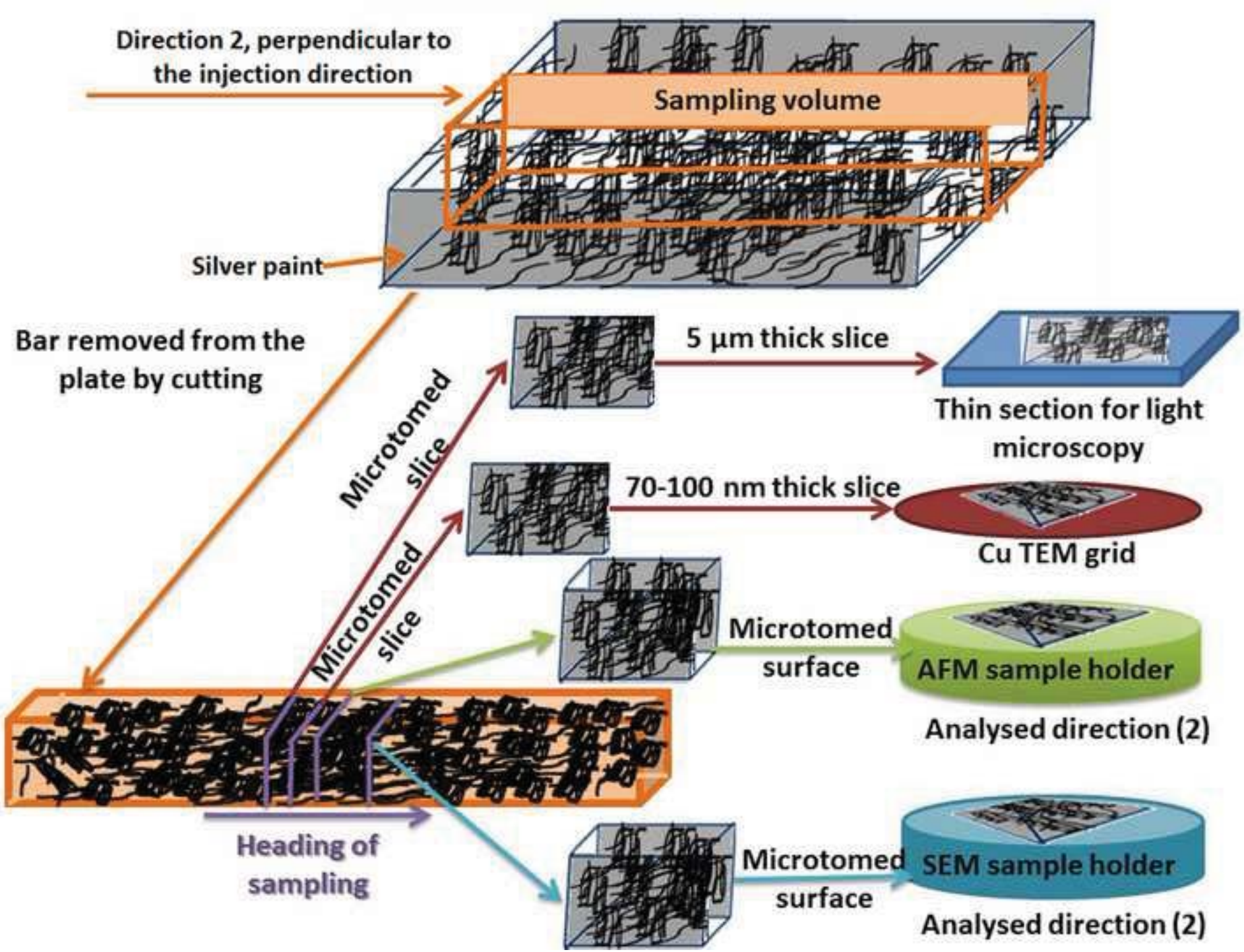

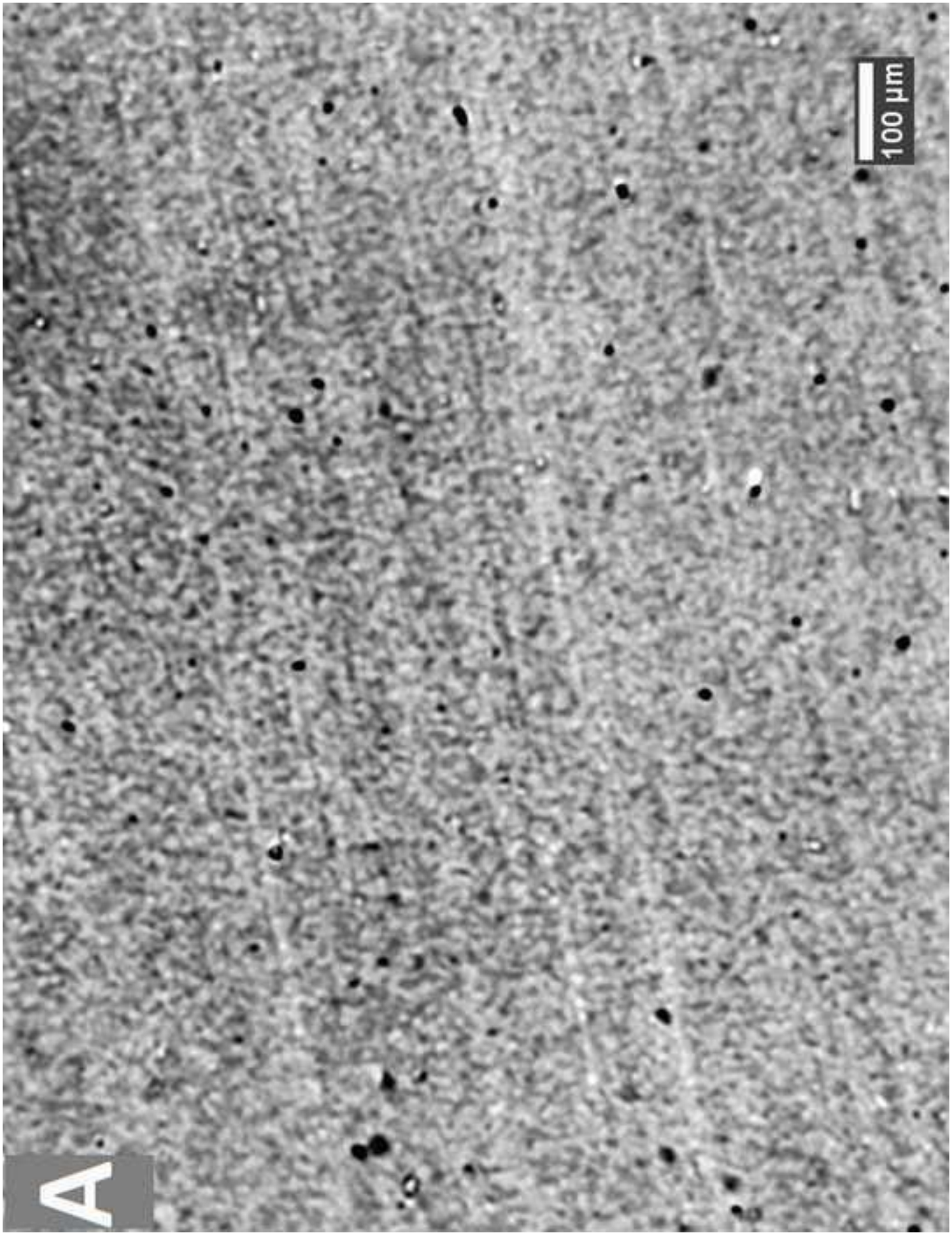

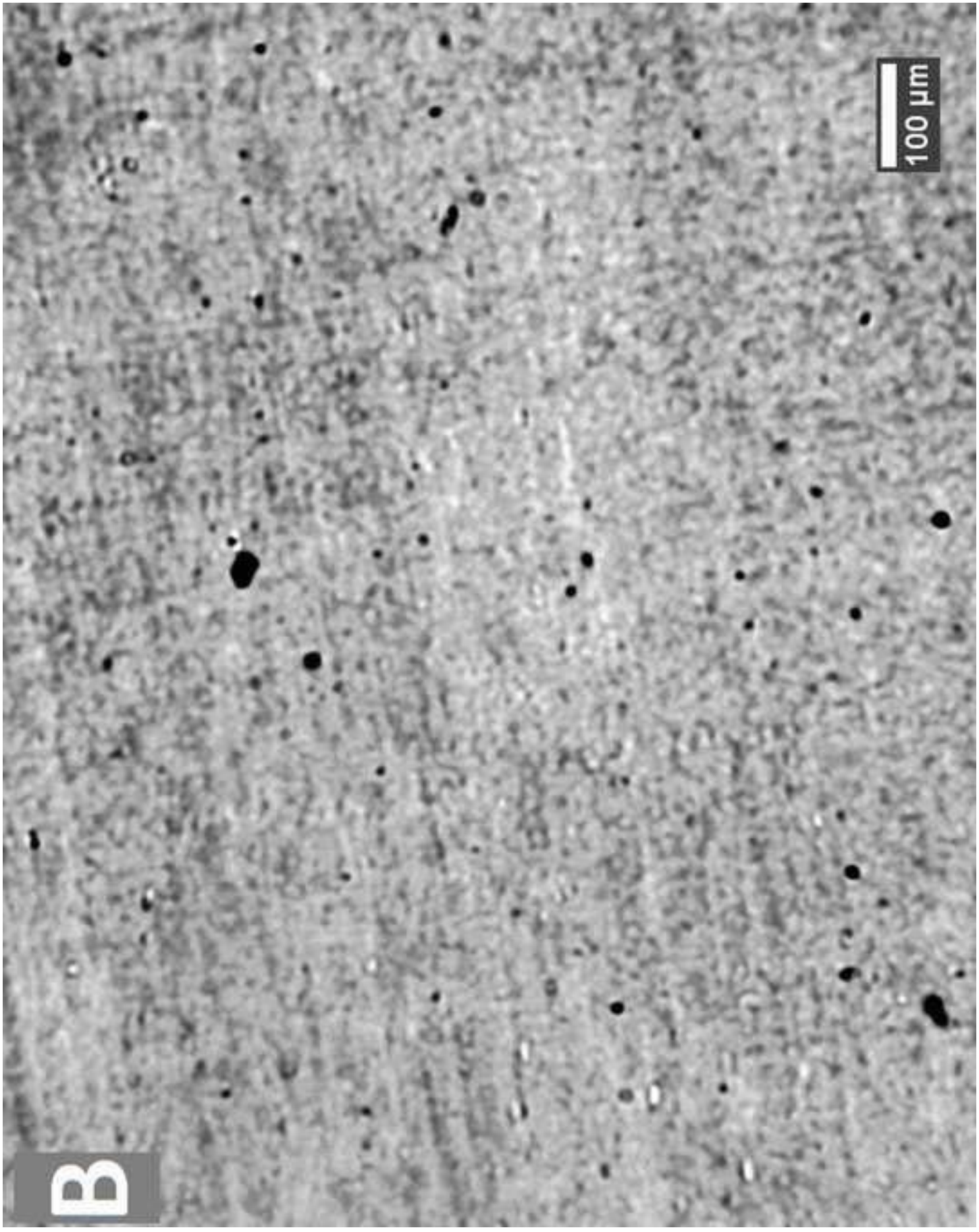

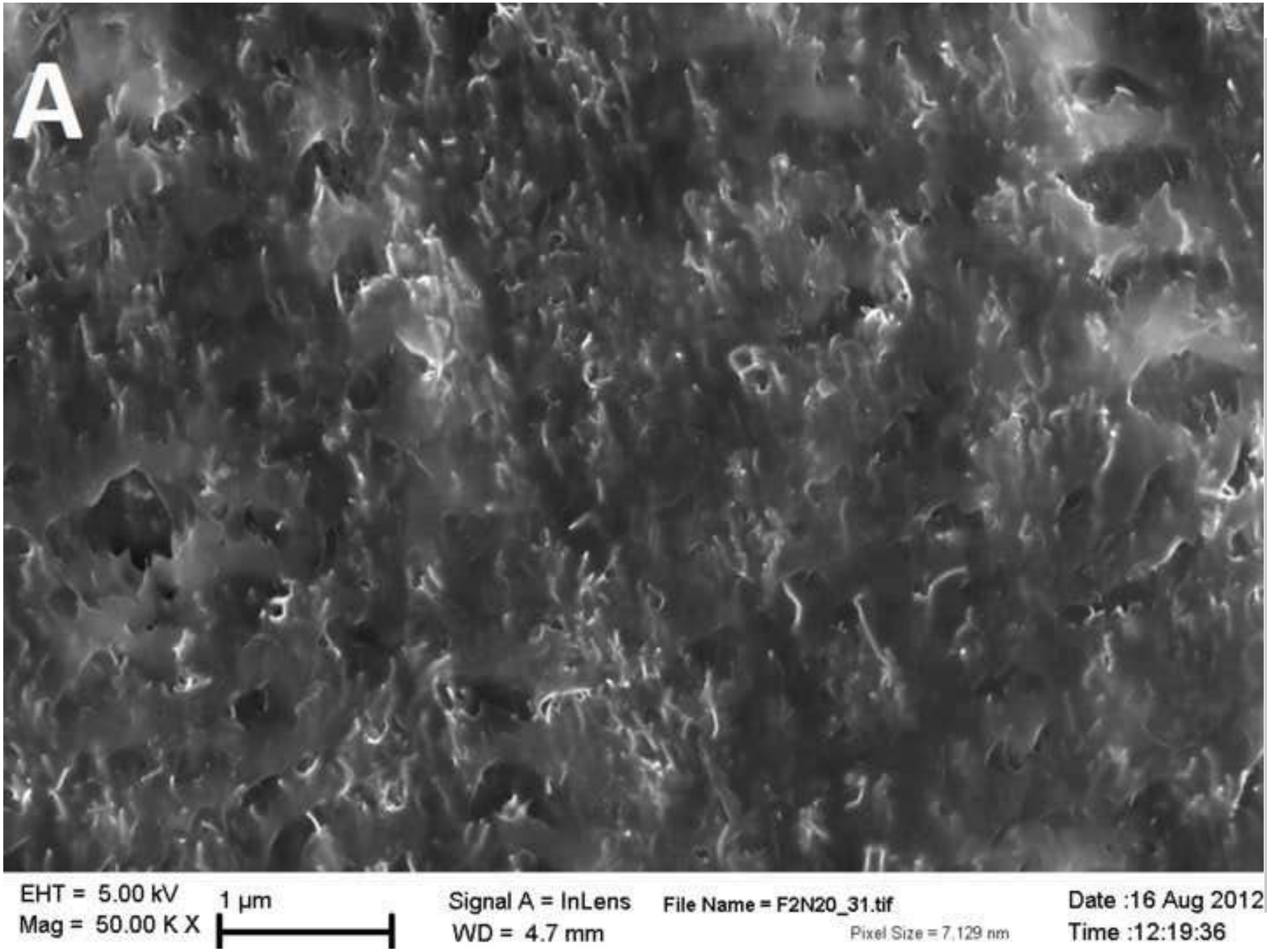

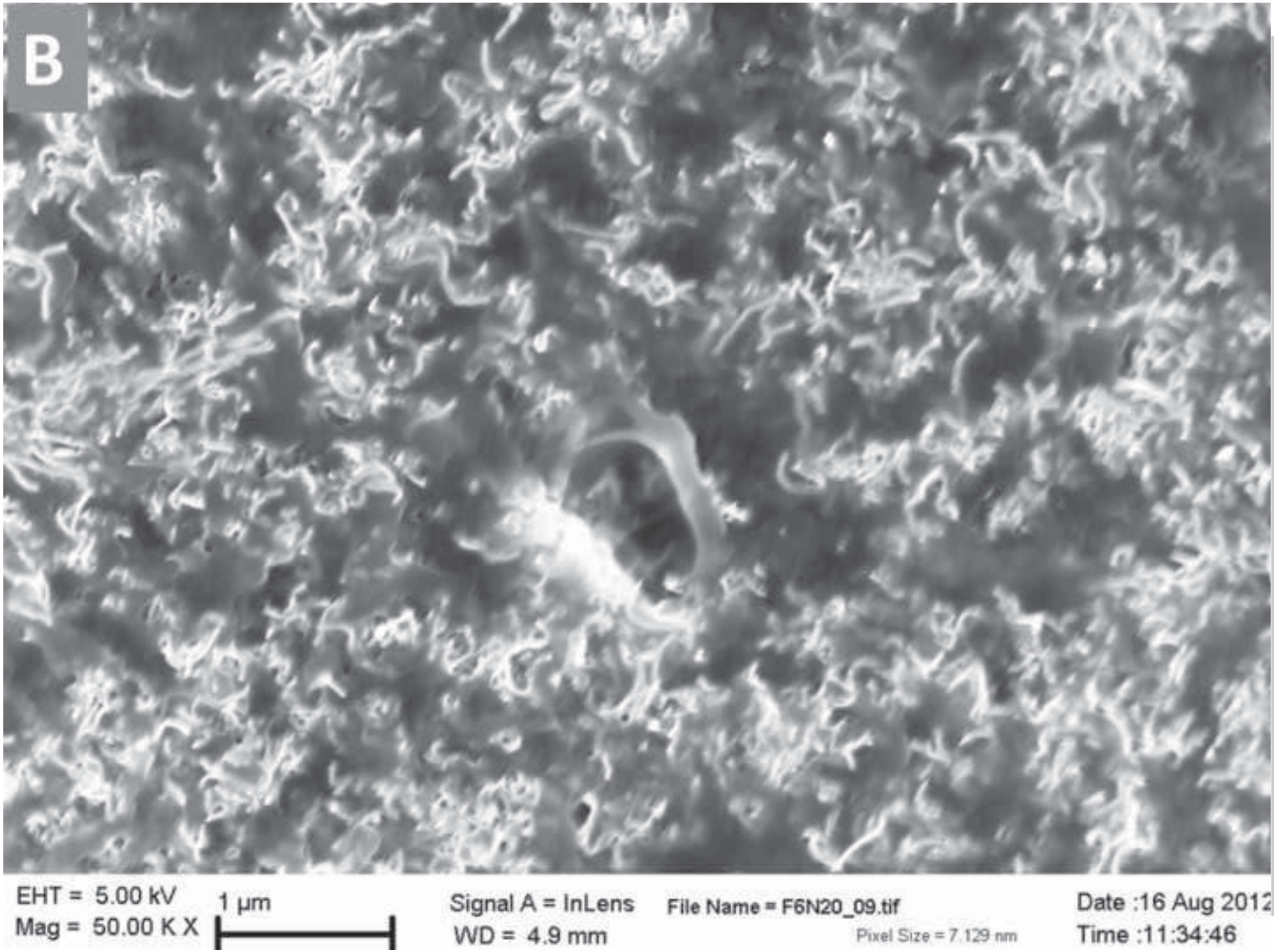

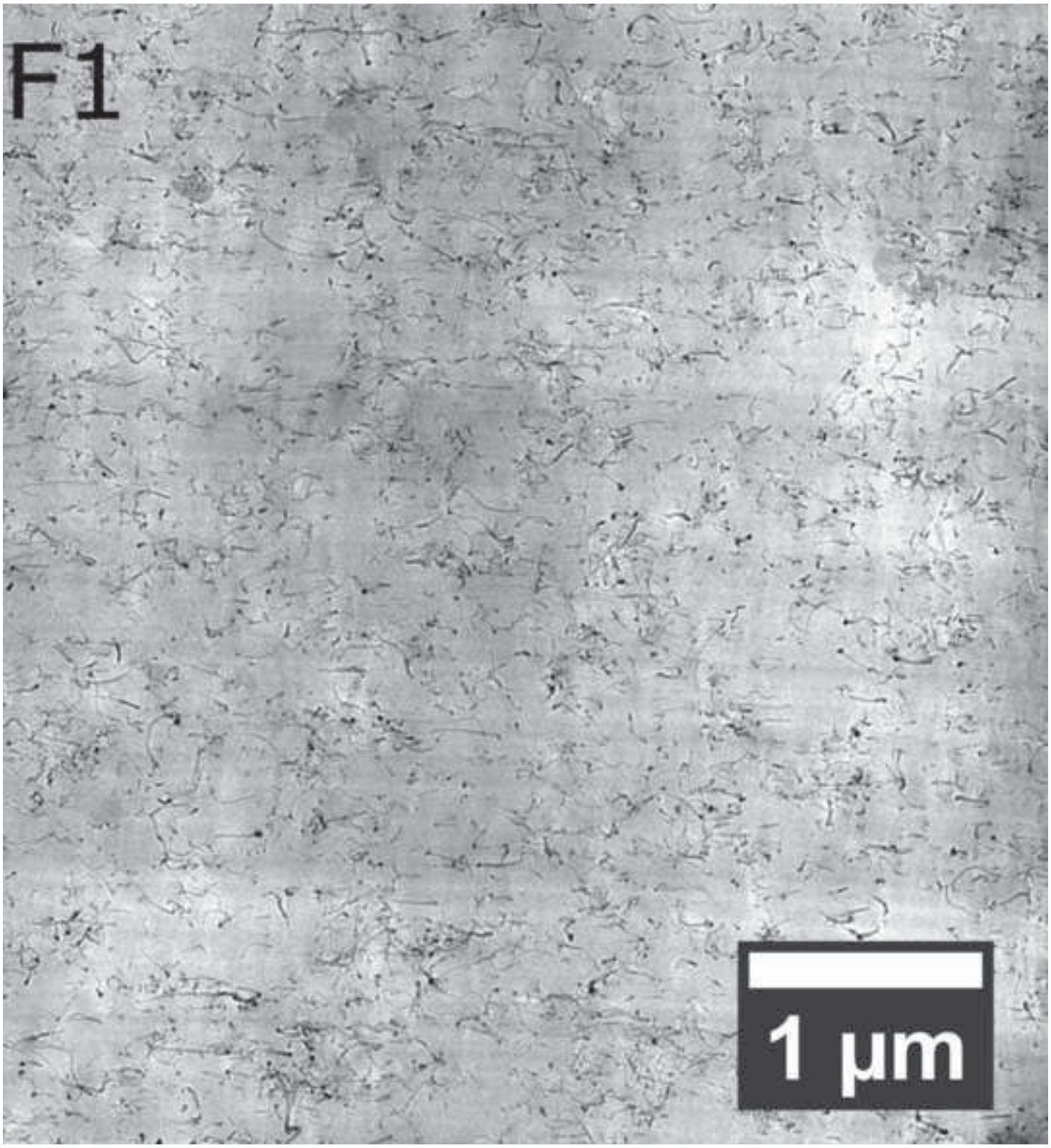

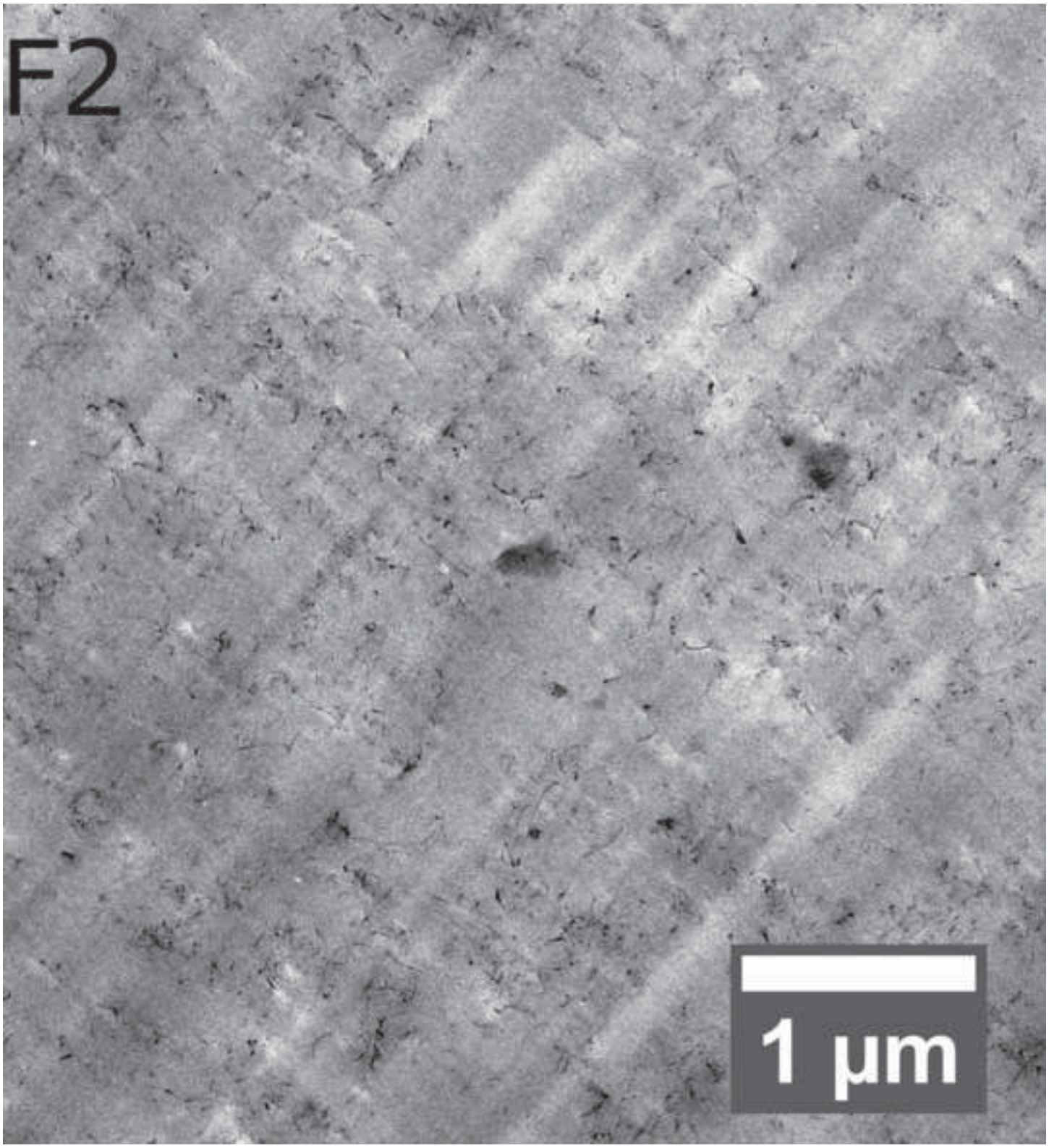
F2
1 µm

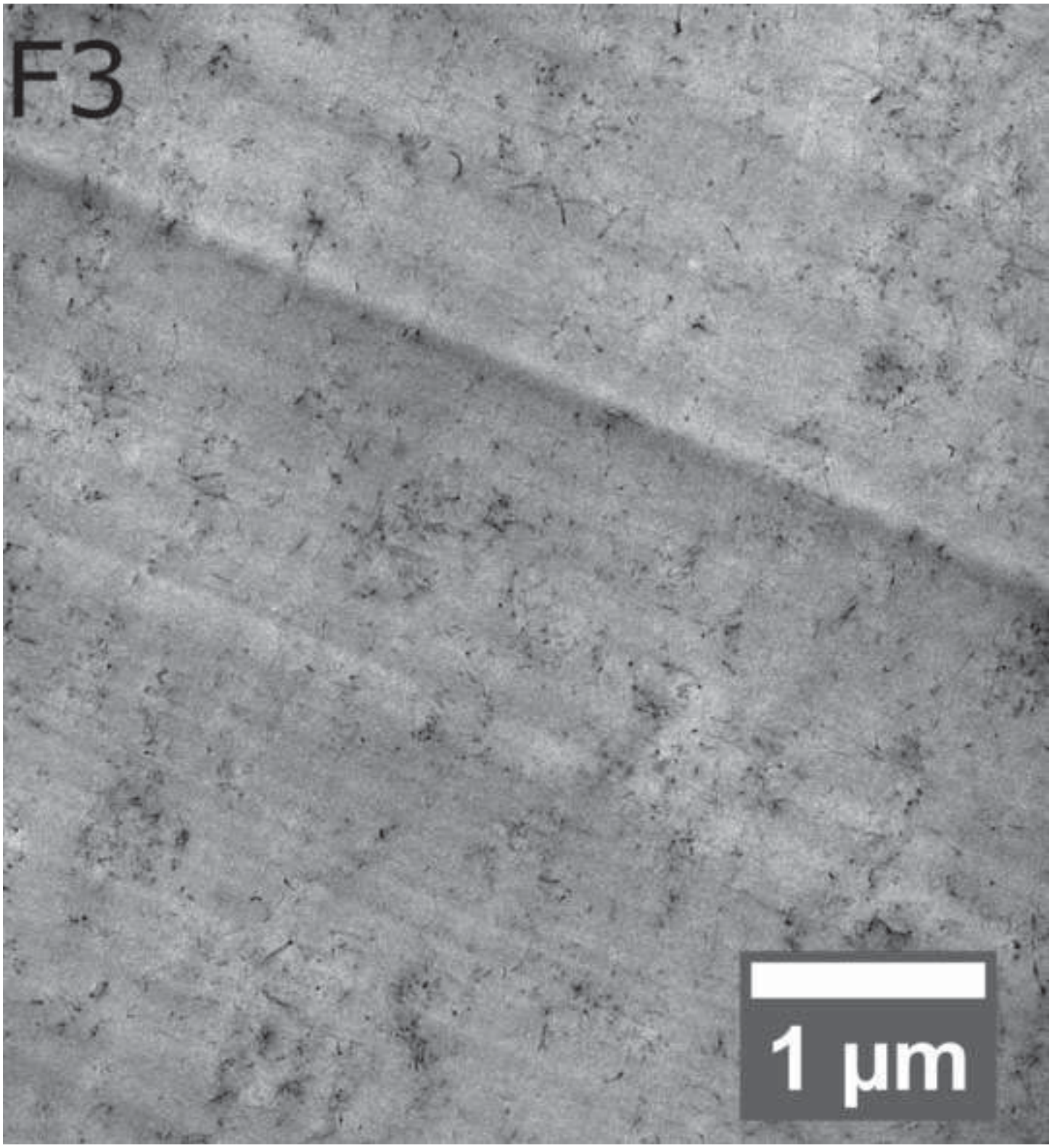

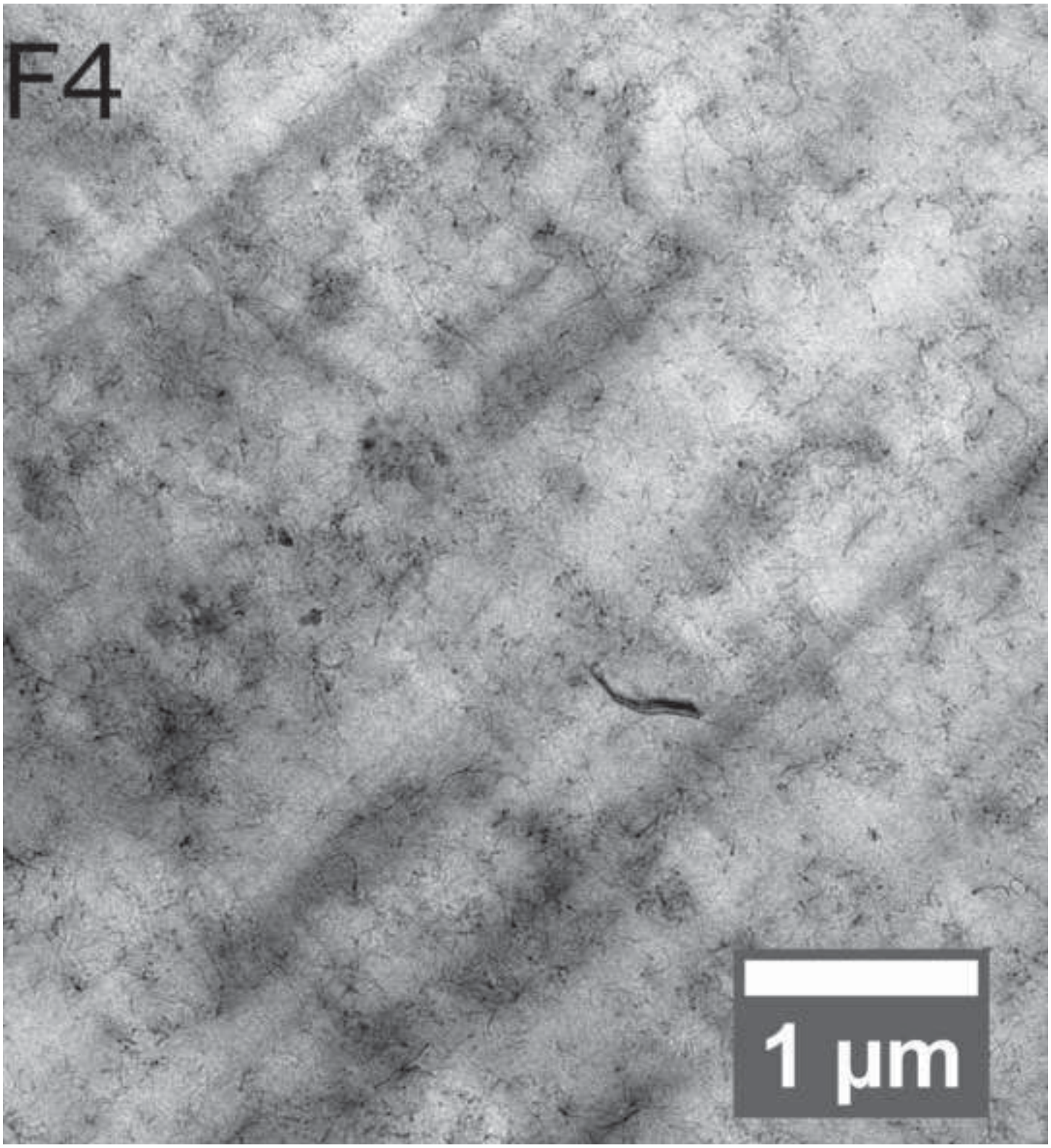

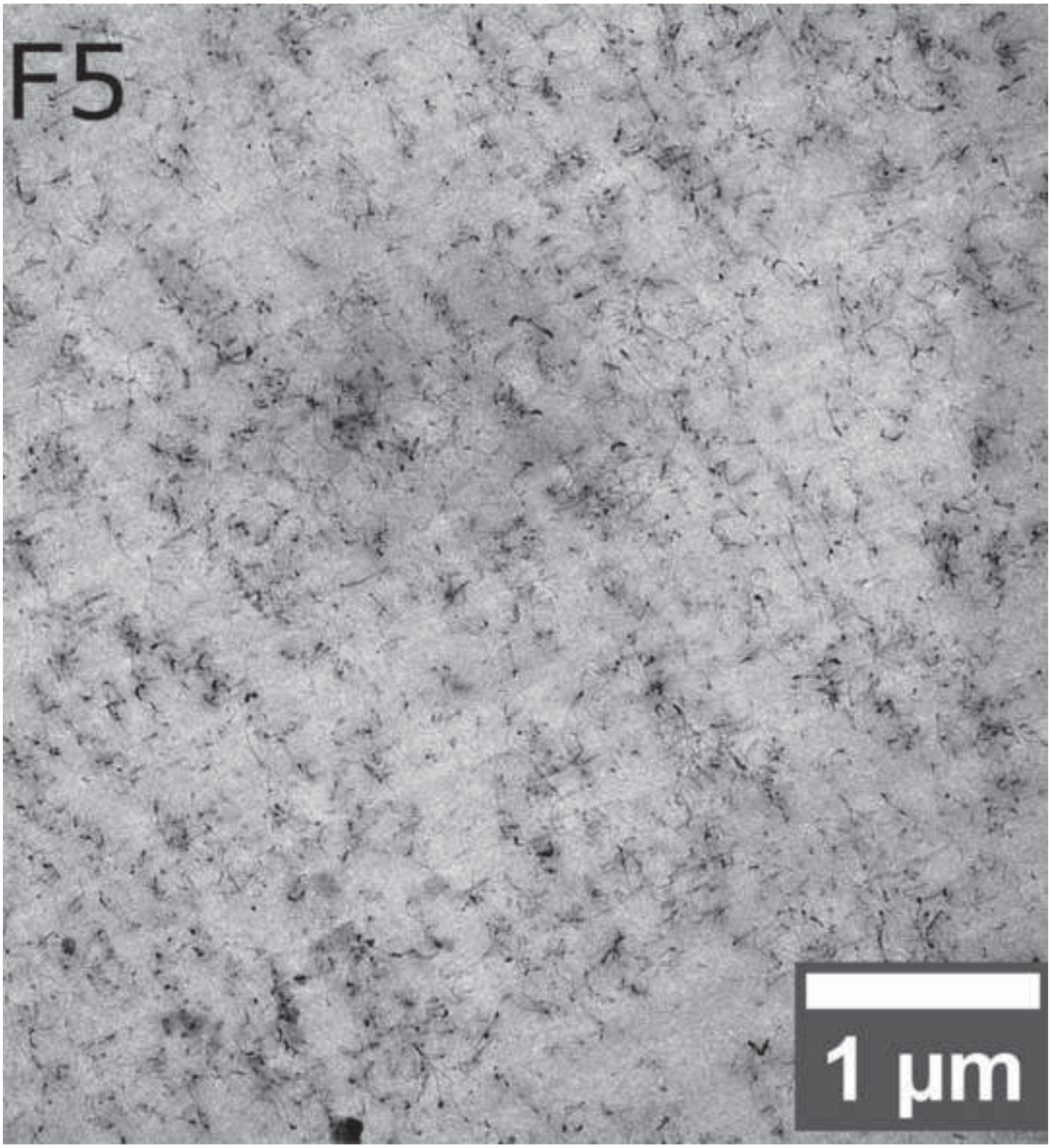
F5
1 µm

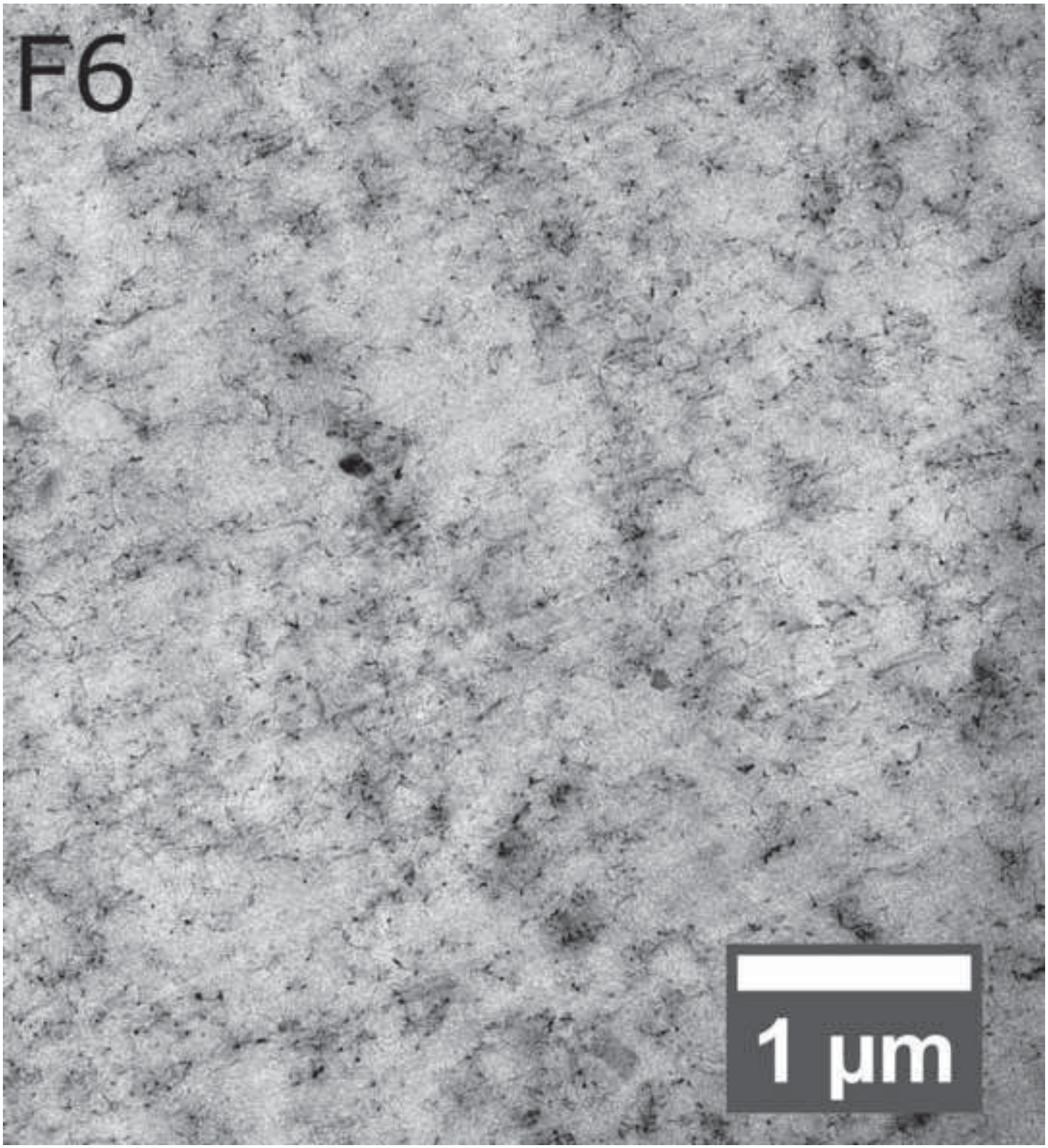
F6
1 µm

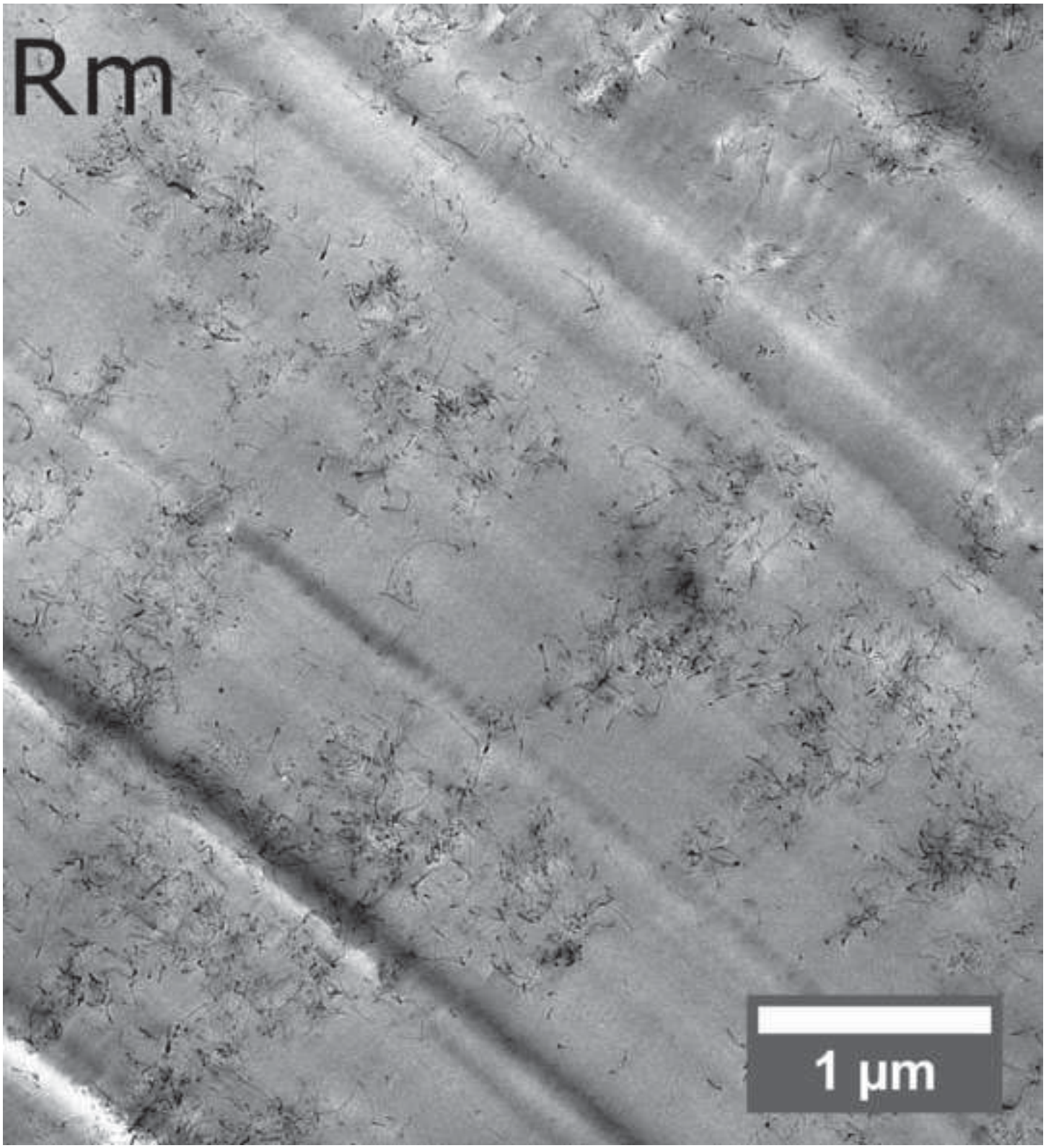

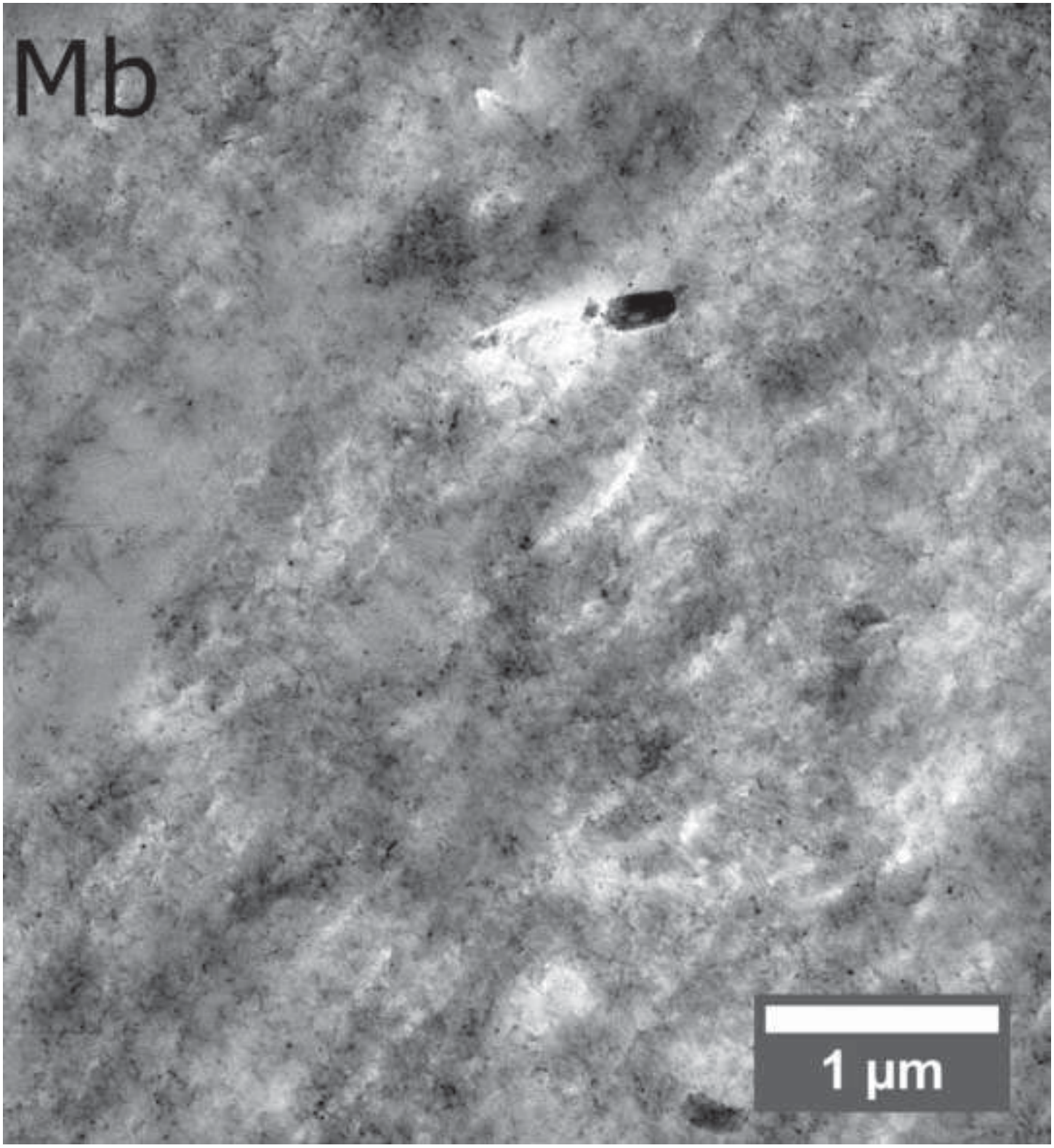

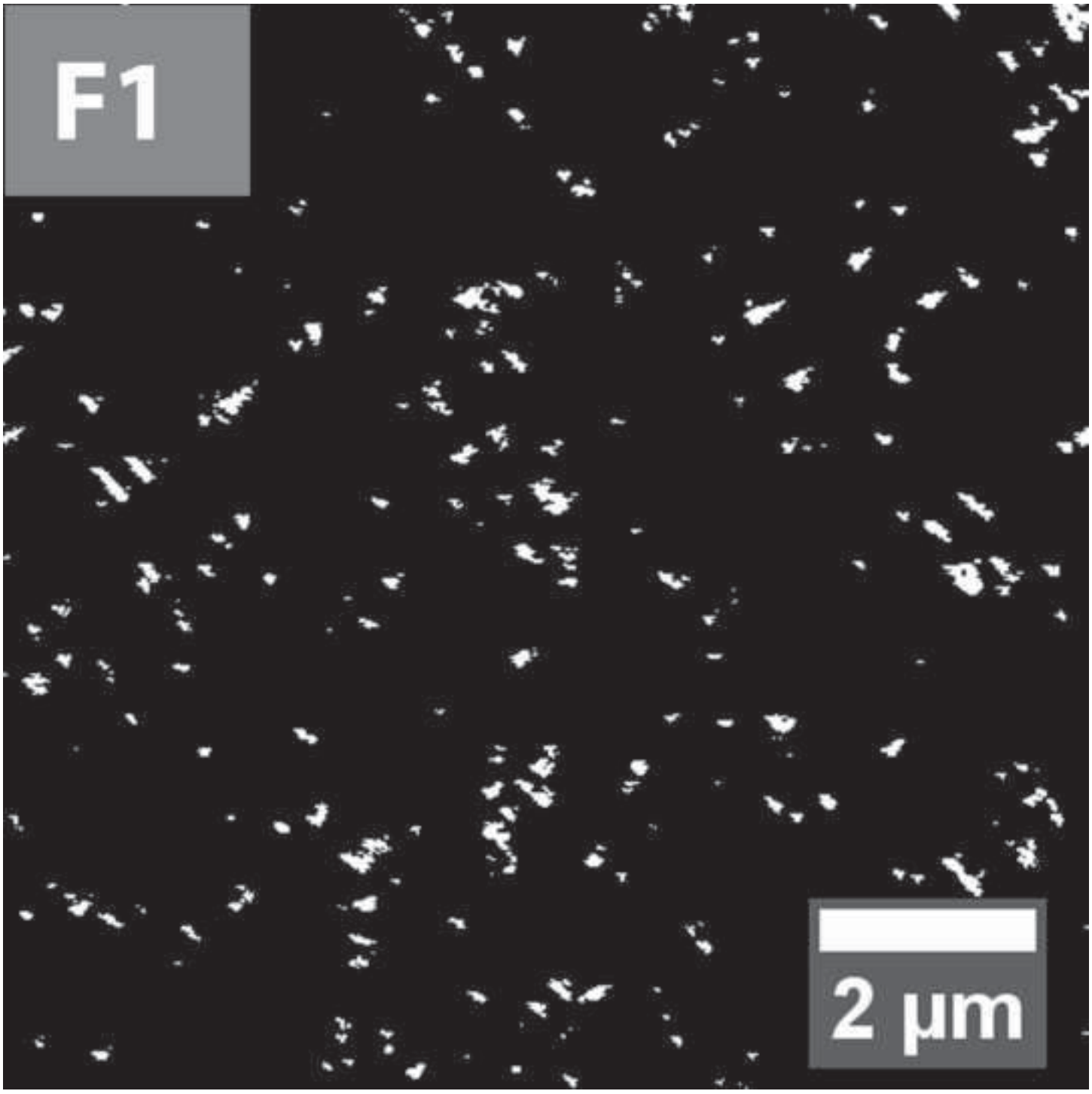
F1
2 µm

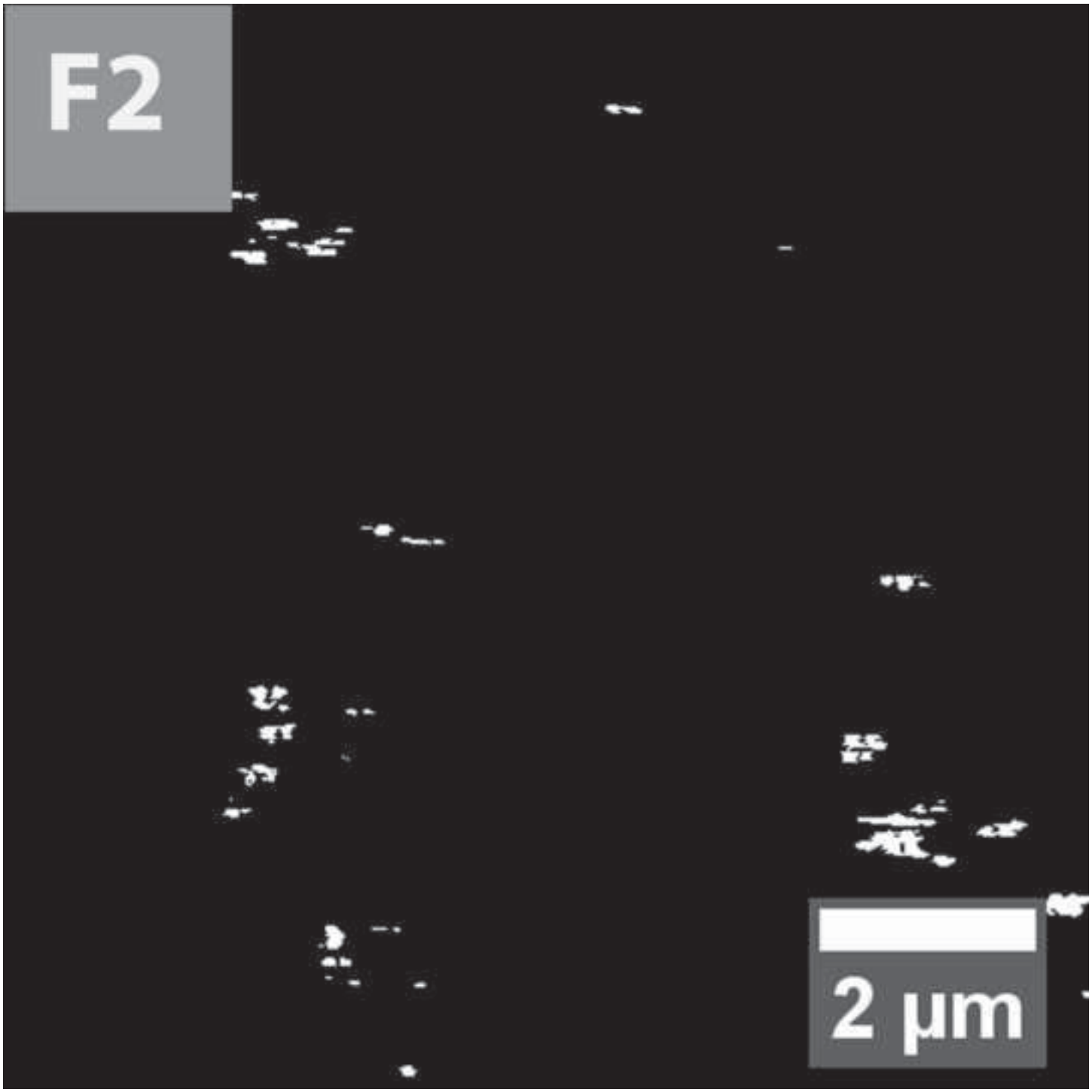

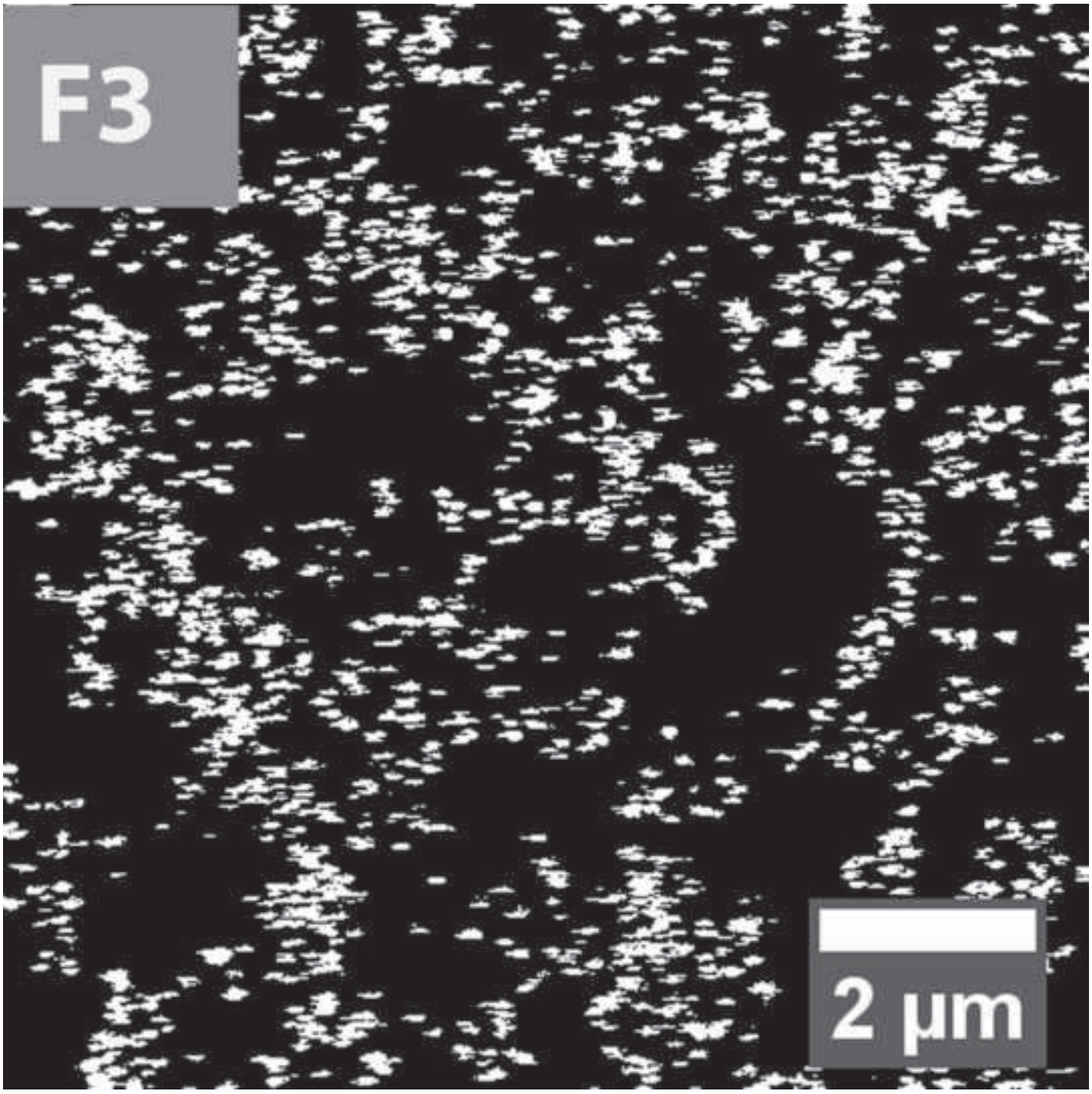
F3
2 µm

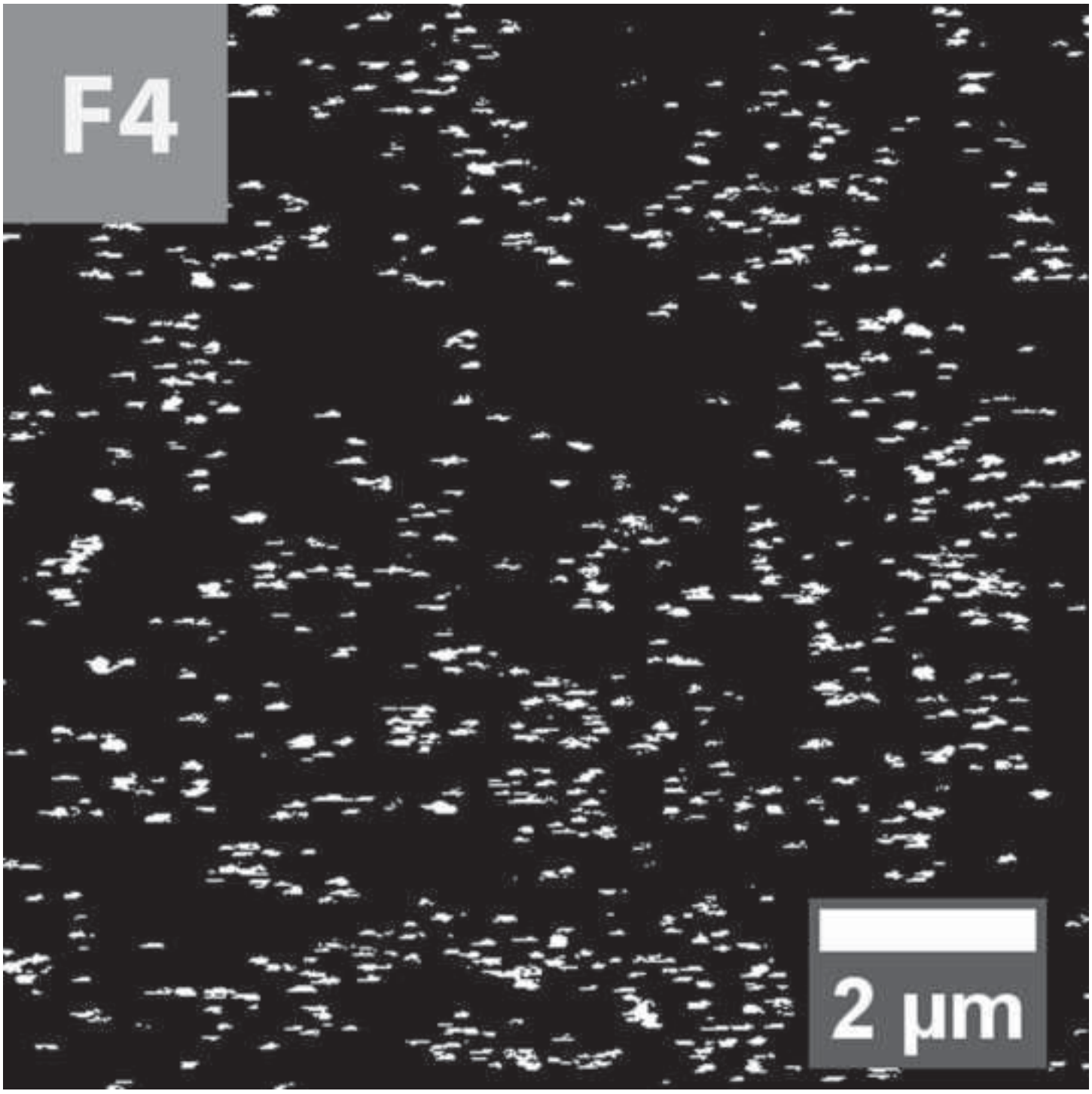
F4
2 µm

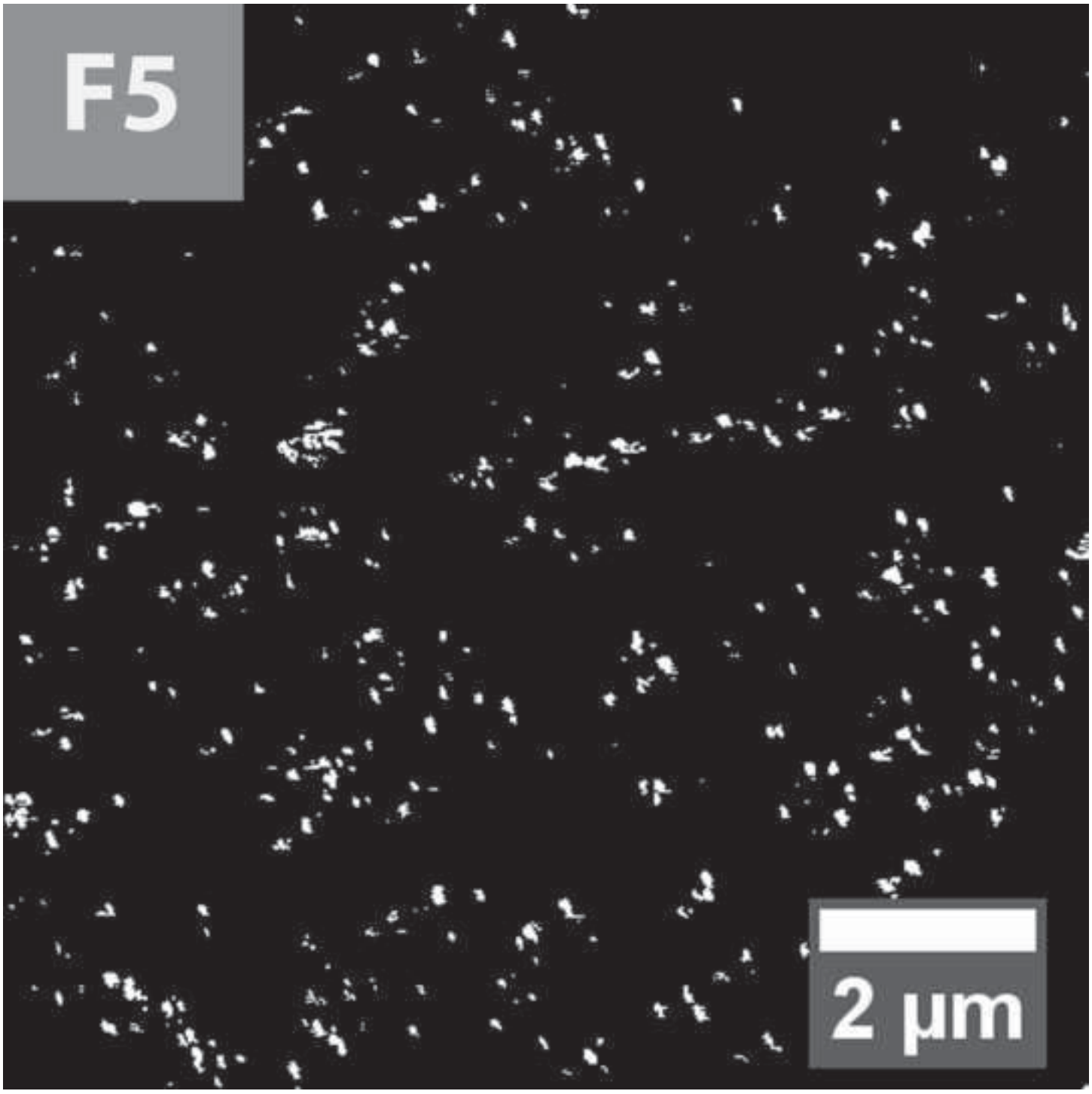
F5
2 µm

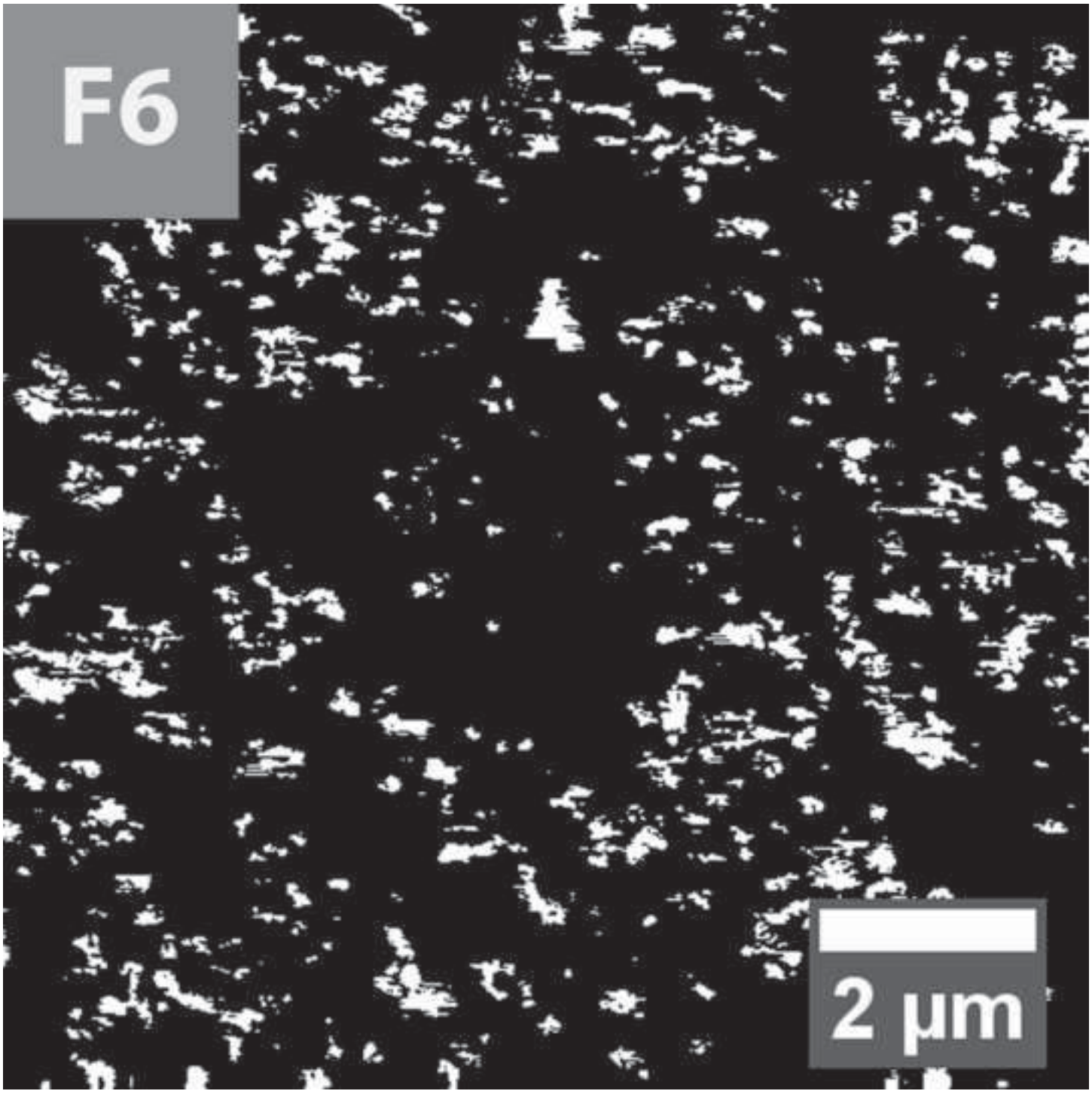
F6
2 µm